

# Noble Metal-free Bimetallic Cobalt/Manganese Oxide Catalyst for Hydrogen Generation by Decomposition of Hydrous Hydrazine

Youngyong Kim and Ki-Young Kwon\*

Department of Chemistry, Gyeongsang National University and RINS, Jinju-si 52828, South Korea.

\*E-mail: kykwon@gnu.ac.kr

Received September 4, 2019, Accepted September 18, 2019

Bimetallic cobalt and manganese oxide (Co/MnO) is prepared by annealing the spinel structure of  $\text{CoMn}_2\text{O}_4$  under hydrogen environment. This noble metal-free catalyst is applied for hydrogen generation from aqueous hydrazine solution. X-ray powder diffraction, transmission electron microscopy, energy-dispersive spectroscopy, and X-ray photoelectron spectroscopy results indicated that the phase separation of metallic cobalt and manganese monoxide from  $\text{CoMn}_2\text{O}_4$  occurs during annealing process. Co/MnO exhibits catalytic activity with the TOF value of  $14.2 \text{ h}^{-1}$  and 100% selectivity without generation of ammonia at 343 K. It is found that metallic cobalt plays role on the active site for hydrogen generation.

**Keywords:** Bimetallic catalyst, Cobalt, Manganese, Hydrogen, Hydrazine

## Introduction

Hydrogen gas is considered as a clean energy source due to no generation of greenhouse gases during combustion process.<sup>1,2</sup> Besides the development of economic and easy hydrogen generation, advanced hydrogen storage materials is essential for implementing hydrogen economy.<sup>3</sup> So far, the liquid hydrogen storage materials are attracting lots of interest due to safe storing under ambient conditions and easy transportation using the existing fuel infrastructure.<sup>4,5</sup> Among these candidates, hydrous hydrazine ( $\text{N}_2\text{H}_4 \cdot \text{H}_2\text{O}$ ) is considered as a promising chemical owing to the high content of hydrogen (8.0 wt %) and the advantage of  $\text{CO}_x$ -free  $\text{H}_2$  production.<sup>6</sup> Hydrazine monohydrate can be decomposed via two pathways and generate different products.<sup>7,8</sup>



To maximize hydrogen generation from hydrazine, the reaction pathway should follow the pathway (1), whereas the unwanted pathway (2) must be avoided. The rare transition metal based catalysts such as Ir,<sup>9</sup> Pt,<sup>10,11</sup> Rh<sup>12,13</sup> have shown the high catalytic activity for hydrazine decomposition in aqueous solution. Previous research efforts have led to the development of bimetallic catalysts, which are primarily composed of noble metal and non-noble transition metal.<sup>10,14–16</sup> For examples, CoIr-supported  $\gamma\text{-Al}_2\text{O}_3$  (TOF:  $27.76 \text{ h}^{-1}$  at  $25^\circ\text{C}$ ),<sup>15</sup> CoPt-supported CeO (TOF:  $194.8 \text{ h}^{-1}$  at  $25^\circ\text{C}$  under 0.5 M NaOH condition),<sup>14</sup> NiPt-MnO<sub>x</sub> supported on NPC-900 (TOF:  $120 \text{ h}^{-1}$  at room temperature)<sup>17</sup> were reported. Here, we reported a cobalt and manganese bimetallic catalyst composed of the phase

separated metallic cobalt and manganese oxide (Co/MnO). It is noteworthy that our sample is a platinum-group metals free catalyst for hydrogen generation from aqueous hydrazine. For comparison, we prepared two additional catalysts which are metallic cobalt and manganese oxide (MnO), respectively. We found that catalytic activity originated from metallic cobalt and MnO acts as a catalytic support of metallic cobalt. Our bimetallic catalyst (Co/MnO) shows higher catalytic activity than monometallic cobalt catalyst. We propose that the improved catalytic property is come from the synergistic electric effect between metallic Co and MnO involved in charge transfer steps.

## Experimental

**Synthesis of Spinel  $\text{CoMn}_2\text{O}_4$  and Co/MnO.**  $\text{CoMn}_2\text{O}_4$  was synthesized by a one-step hydrothermal method. An aqueous 10 mL of 10 M NaOH was added into 50 mL of aqueous solution containing  $\text{Co}(\text{NO}_3)_2 \cdot 6\text{H}_2\text{O}$  (1 mmol) and  $\text{Mn}(\text{ClO}_4)_2$  (2 mmol). After stirring above solution at room temperature for 10 min, the mixture was transferred into a Teflon-lined autoclave reactor and kept at  $160^\circ\text{C}$  for 6 h. Black-green precipitates were collected by centrifugation and washed three times with DI water followed by drying the sample under vacuum for overnight. Finally, the metallic cobalt and manganese monoxide (Co/MnO) was obtained by annealing  $\text{CoMn}_2\text{O}_4$  at  $500^\circ\text{C}$  for 3 h under hydrogen gas condition (4%  $\text{H}_2$ , 96% Ar). For comparison, monometallic Co, and MnO were prepared by the same procedures as mentioned above by adding one metal precursor [either  $\text{Co}(\text{NO}_3)_2 \cdot 6\text{H}_2\text{O}$  or  $\text{Mn}(\text{ClO}_4)_2$ ].

**Characterization.** X-ray diffraction patterns were recorded using a Bruker D8 Advance X-ray diffractometer (Billerica, MA, USA), with Cu  $K_\alpha$  radiation. The X-ray

photoelectron spectroscopy (XPS) results were obtained on a X-ray photoelectron spectrometer K-Alpha (Thermo Scientific, Tokyo, Japan) in which monochromated Al  $K_{\alpha}$  radiation ( $h\nu = 1486.6$  eV) is illuminated as the light source. The X-ray anode was run at 25 W and the voltage was maintained at 15 kV. The pass energy was fixed at 23.5 eV to ensure sufficient resolution to determine peak positions accurately. The binding energies were calibrated by using the C 1 s peak at 284.8 eV. The morphologies of samples were characterized by transmission electron microscopy (TEM, Tecnai G2 F20S-TWIN, FEI, USA). The composition of the sample was analyzed by energy-dispersive spectroscopy (EDS) fitted on the TEM. ICP-AES was performed to determine the composition of Co/MnO catalyst.

**Catalytic Tests.** The catalytic dehydrogenation from hydrazine monohydrate was tested in a two-necked round-bottom test tube, where one neck was connected to a gas burette to measure the volume of the released gas, other neck was used to inject hydrazine monohydrate. The reaction temperature (70 °C) was controlled using water bath. The reaction was initiated by injecting 5 mL of  $N_2H_4 \cdot H_2O$  solution (0.12 mol/L) into the test tube containing 10 mg of catalyst. The volume of generated gas was measured using a gas barrette after either passing or bypassing a 1.0 M HCl trap. Hydrazine conversion ( $X_{N_2H_4}$ ) was calculated by ratio of the generated volume of the gas to the theoretical total volume of gas if the hydrazine is totally decomposed to  $N_2$  and  $H_2$ . Turnover frequency (TOF) is calculated at 50% hydrazine conversion as following equation.<sup>15</sup>

$$TOF = (PV/RT)/(3n_{Metal}t)$$

Here,  $P$  is the atmospheric pressure,  $V$  is the volume of generated gases ( $H_2 + N_2$ ),  $R$  is universal gas constant,  $T$  is the reaction temperature,  $n_{Metal}$  is the mole number of metal in catalyst, and  $t$  is the reaction time for the 50% conversion of hydrazine monohydrate.

## Results and Discussion

**Structural Characteristics.** Figure 1 showed the X-ray powder diffraction (XRD) patterns of the precipitates before and after annealing. For the precipitates before annealing, the dominant spinel structure of  $CoMn_2O_4$  (JCPDS No.01-077-0471)<sup>18,19</sup> as well as small amount of  $CoO(OH)$  (JCPDS No.01-072-2280) was presented. It was known that the  $CoO(OH)$  can be formed under the strong aqueous basic solution.<sup>20,21</sup> After being annealed under hydrogen gas environment (4%  $H_2/96\%$  Ar) at 500 °C for 3 h, the XRD patterns of the  $CoMn_2O_4$  was dramatically changed into a simplified form which assigned to MnO (JCPDS No.00-007-0230) and metallic Co (JCPDS No.00-001-1255) (Figure 1(b)). This indicates that the mixed phases containing  $CoO(OH)$ , and  $CoMn_2O_4$  reduced to metallic Co and MnO under hydrogen treatment at 500 °C. While diffraction angles of metallic cobalt are exactly matched with literature data,<sup>22</sup> the two theta values of MnO

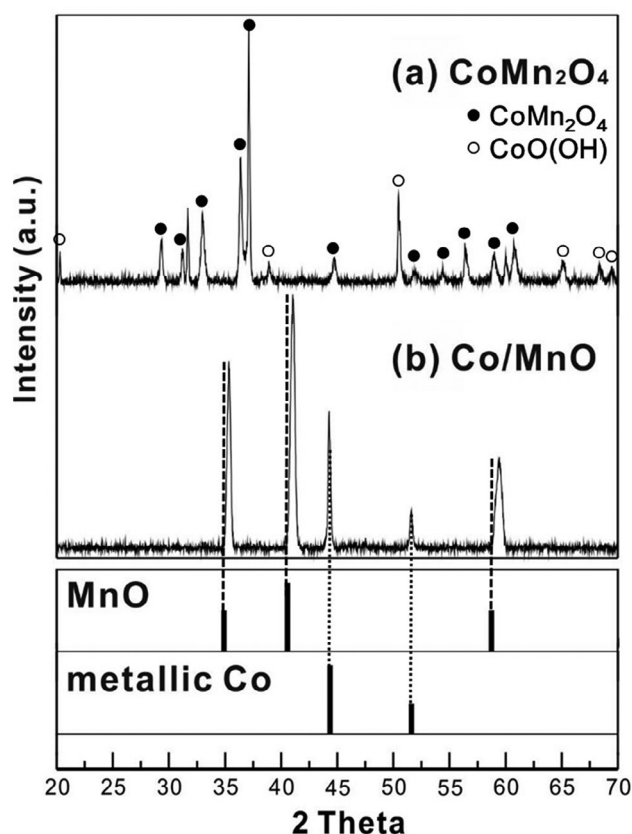
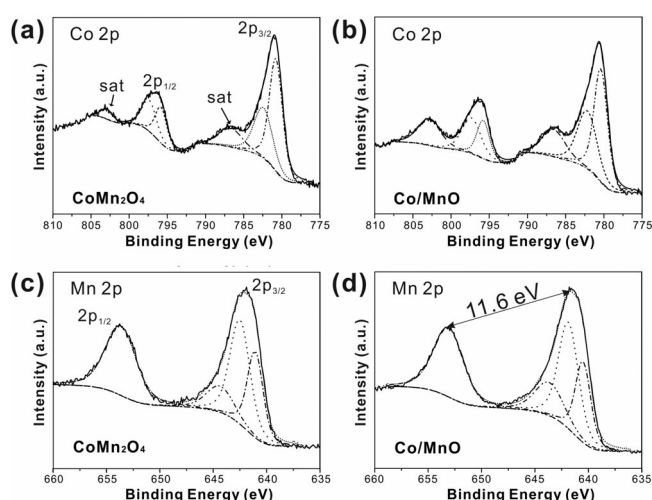


Figure 1. XRD patterns of  $CoMn_2O_4$  (a) and Co/MnO (b).

shift toward approximately 0.4–0.6 higher angle. The shift of diffraction angles to positive value and decreased lattice parameters of MnO was previously reported when  $Mn^{2+}$  ions [ $r_{ion}(Mn^{2+}) = 0.83$  Å] are substituted to smaller  $Co^{2+}$  ions [ $r_{ion}(Co^{2+}) = 0.745$  Å].<sup>23</sup> Therefore, we think that the small amounts of  $Co^{2+}$  ions still remain in MnO during phase segregation process from the spinel structure of  $CoMn_2O_4$  into metallic cobalt and MnO.

Figure 2 showed the XPS spectra to characterize the chemical nature of the Co, Mn, and O and investigate the effect of hydrogen treatment of the sample in annealing process. The Co 2p spectra of  $CoMn_2O_4$  can be deconvoluted by six species composing two pairs of spin-orbital doublets characteristic of  $Co^{2+}$  and  $Co^{3+}$  and two shake-up satellite, which are denoted “sat” (Figure 2(a)). Two Co 2p<sub>3/2</sub> and Co 2p<sub>1/2</sub> peaks located at around 780.6 and 796.2 eV are accompanied by two major shake-up satellite peaks (around 786.6 and 803 eV) in Figure 2(a) and (b), suggesting the abundant presence of the  $Co^{2+}$  in  $CoMn_2O_4$  and Co/MnO. Particularly, the intensity of satellite peaks of Co/MnO is higher than that of  $CoMn_2O_4$ . It was reported that the enhancement satellite intensity around 786 eV indicates the presence of Co with the oxidation state of +2. Therefore, we believe that the cobalt atoms on the surface of Co/MnO are mostly oxidized to  $Co^{2+}$  forming thin CoO shell at ambient condition although XRD patterns showed only the presence of zerovalent oxidation state.<sup>25</sup> The Mn 2p XPS



**Figure 2.** X-ray photoelectron spectra for the  $\text{CoMn}_2\text{O}_4$  and  $\text{Co/MnO}$ . (a) Co 2p XPS spectrum of the  $\text{CoMn}_2\text{O}_4$ , (b) Co 2p XPS spectrum of the  $\text{Co/MnO}$ , (c) Mn 2p XPS spectrum of the  $\text{CoMn}_2\text{O}_4$ , and (d) Mn 2p XPS spectrum of the  $\text{Co/MnO}$ .

spectrum of  $\text{CoMn}_2\text{O}_4$  exhibits two major peaks at binding energies of 642.0 and 653.8 eV which correspond to Mn  $2p_{1/2}$  and Mn  $2p_{3/2}$ , respectively. After being annealed, the two signals of Mn  $2p_{3/2}$  and  $2p_{1/2}$  centered at 641.6 and 653.2 eV which correspond to the shift to approximately 0.4–0.6 lower energy. These result suggested that Mn with oxidation state of  $3+/4+$  reduced to  $\text{Mn}^{2+}$  during an annealing process under hydrogen condition.<sup>26</sup> In addition, the spin energy separation between Mn  $2p_{1/2}$  and Mn  $2p_{3/2}$  is 11.6 eV. This value is commonly referred to represent the oxidation state of  $\text{Mn}^{2+}$ .<sup>27</sup>

TEM and EDX experiments (Figure 3) were applied to characterize the morphology and elemental composition of the  $\text{CoMn}_2\text{O}_4$  and  $\text{Co/MnO}$ . Figure 3(a) represents the TEM image of  $\text{CoMn}_2\text{O}_4$ , which is rhombus shape.

EDX data of  $\text{CoMn}_2\text{O}_4$  (Figure 3(a)–(e)) indicates that Mn and Co are well dispersed in the entire area of  $\text{CoMn}_2\text{O}_4$  crystallites. After annealing the  $\text{CoMn}_2\text{O}_4$  at 500 °C for 3 h under hydrogen atmosphere, the rhombus shape of  $\text{CoMn}_2\text{O}_4$  was changed into formless morphology which is composed of round shape darker particles and less darker framework (Figure 3(f)). Importantly, EDX analyses demonstrated that cobalt is abundant in round shape particles, and manganese is abundant in shapeless framework. Figure 3(g) shows the enlarged TEM image of the area marked by the red square in Figure 3(b). Figure 3(h)–(k) represents the elemental mapping images of  $\text{Co/MnO}$ . While Co is mainly located in the particle (in comparison with Figure 3(i)), Mn is placed in the framework (Figure 3(i)). Therefore, we assigned that the particle and framework correspond to metallic cobalt and MnO, respectively. It should be noticed that there is certain amount of cobalt in framework although majority amount of cobalt exist in particle. EDX Quantification indicated that the ratio of cobalt to manganese is approximately 10%. The presence of

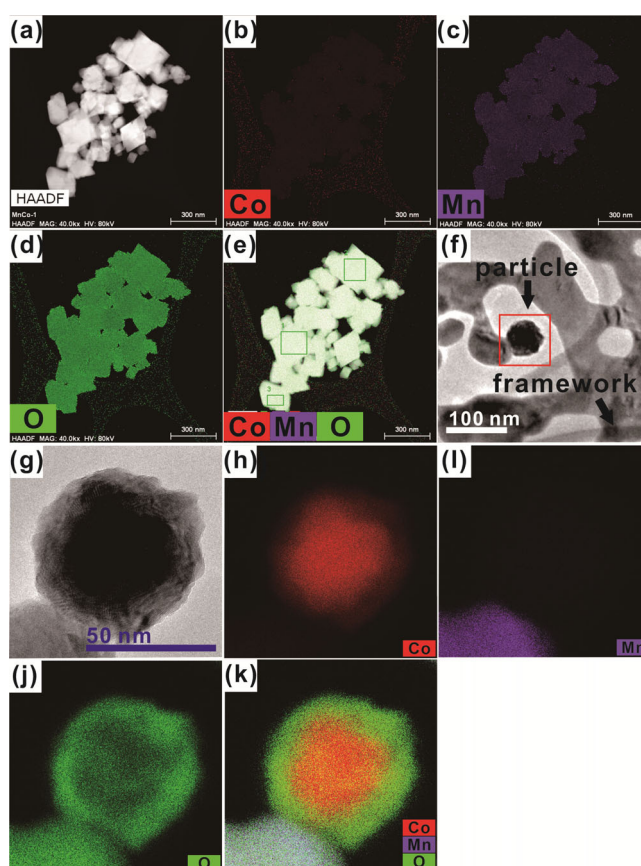


**Figure 3.** TEM image and EDS element mapping images of the  $\text{CoMn}_2\text{O}_4$  and the  $\text{Co/MnO}$ . The HAADF image of (a)  $\text{CoMn}_2\text{O}_4$ , and EDS maps of the (b) cobalt (red), (c) manganese (purple), (d) oxygen (green), and (e) overlapping of Co, Mn, and O, TEM images of (f)  $\text{Co/MnO}$ , (g) TEM image of boxed region in (f) and corresponding EDS maps of the (h) cobalt (red), (i) manganese (purple), (j) oxygen (green), and (k) overlapping of Co, Mn, and O.

cobalt in framework (assigned to MnO) well matched with the XRD pattern shift of MnO toward higher angle which originated from incorporation of smaller size of cobalt ion than that of manganese ion. Oxygen is distributed in both the particle and framework (Figure 3(j)). Particularly, in particle, oxygen is sparse in the core area while dense in the outer area. This result seems to be the oxidation of the surface of metallic cobalt in the air. This surface oxidation phenomena of cobalt is supported by the presence of  $\text{Co}^{2+}$  in XPS data shown in Figure 2. However, the presence of any cobalt oxide such as CoO does not appear in XRD data (Figure 1). Therefore, we concluded that the thickness of oxide layers in cobalt nanoparticles is very thin or the oxide layers exhibit amorphous phase. In framework, oxygen and cobalt are evenly distributed in entire area indicating the presence of MnO. Figure 3(k) represent the elemental mapping with Co, Mn, and O overlaid. We clearly reconfirmed the presence of oxide layer on the outer shell of cobalt particles (Figure 3(k)). From these results, we conclude that

metallic cobalt and MnO containing 10% cobalt are formed from mainly the spinel structures of  $\text{CoMn}_2\text{O}_4$  through annealing process under hydrogen environment.

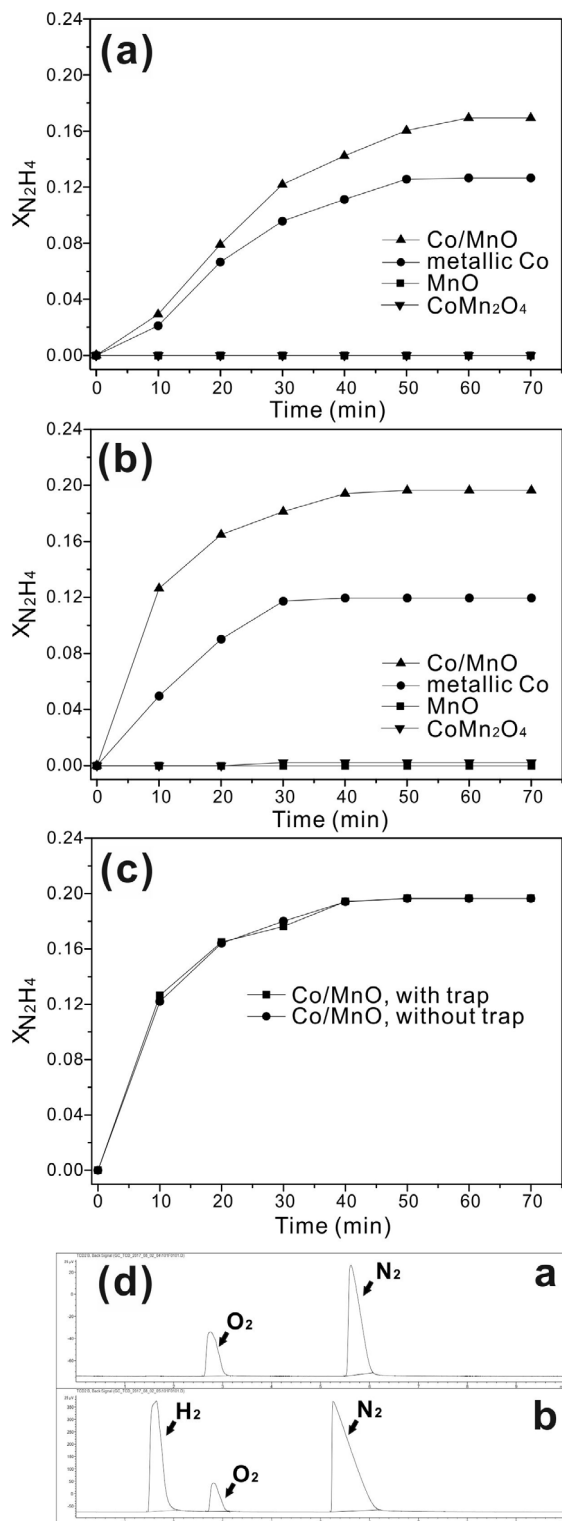


**Figure 4.**  $\text{N}_2\text{H}_4$  conversion as a function of time over the prepared samples at different concentration of NaOH (a) 0 M NaOH, (b) 0.12 M NaOH, (c) 0.12 M NaOH using the co/MnO with/without ammonia trap, and (d) GC profile for gas product of (c).

**Catalytic Performances.** Hydrazine decomposition experiments were carried out to confirm the catalytic activities for hydrogen generation. Figure 4(a) and (b) exhibits the hydrazine conversion ( $X_{\text{N}_2\text{H}_4}$ ) as a function of reaction time using bimetallic catalysts ( $\text{CoMn}_2\text{O}_4$ ,  $\text{Co/MnO}$ ) and monometallic catalysts (metallic Co, MnO) in absence and presence of NaOH, respectively. While the  $\text{Co/MnO}$  and metallic Co showed catalytic activity, the  $\text{CoMn}_2\text{O}_4$  and MnO exhibited almost no catalytic performance. Therefore, we concluded that metallic cobalt plays as an active site for hydrazine decomposition. Interestingly,  $\text{Co/MnO}$  (TOF:  $4.7 \text{ h}^{-1}$ ) exhibit higher catalytic activity than unimetallic Co (TOF:  $\text{h}^{-1}$ ) when the same amount of catalysts are used. This phenomenon can be considered that MnO in the catalyst plays role in promoting the catalytic activity. Xia *et al.* reported the decomposition of hydrazine using NiPt nanoparticles/ $\text{MnO}_x$  in which the ratio of NiPt to  $\text{MnO}_x$  significantly affect the catalytic activity.<sup>17</sup> Recently,  $\text{Co/MnO}$  or  $\text{CoO/MnO}$  are applied for the anode material for lithium-ion batteries where the morphology of metallic cobalt and electrical properties are significantly dependent on the molar ratio of precursor cobalt ions to manganese ions.<sup>28,29</sup> In addition, it is known that charge transfer step in decomposition of hydrazine is important in determining reaction kinetics.<sup>17</sup> Therefore, we believe that optimal electronic structures of  $\text{Co/MnO}$  has superior kinetic property compared to Co.

To study the effect of pH on the rate of hydrazine decomposition, the reaction was carried out under 0.12 M NaOH solution (Figure 4(b)). The catalytic activities of  $\text{Co/MnO}$  and metallic Co are improved approximately three times in the presence of NaOH. It was reported that  $\text{OH}^-$  ions in hydrazine solution decrease the concentration of undesirable  $\text{N}_2\text{H}_5^+$  ( $\text{N}_2\text{H}_5^+ + \text{OH}^- \rightarrow \text{N}_2\text{H}_4 + \text{H}_2\text{O}$ ) acting as promoters.<sup>30</sup> The TOF of the  $\text{Co/MnO}$  and metallic Co in presence of 0.12 M NaOH exhibit 14.2,  $2.5 \text{ h}^{-1}$ , respectively. These value is comparable to the previous noble metal-free catalysts ( $\text{Ni}_{0.5}\text{Fe}_{0.5}$  ( $3.2 \text{ h}^{-1}$  at  $70^\circ\text{C}$ ),<sup>31</sup>  $\text{Ni}_{0.60}\text{Pd}_{0.40}$  ( $5.5 \text{ h}^{-1}$  at  $70^\circ\text{C}$ ),<sup>32</sup>  $\text{Ni}_{50}\text{Fe}_{50}\text{-CT}$  ( $9 \text{ h}^{-1}$  at  $70^\circ\text{C}$ ),<sup>33</sup>  $\text{Ni}_{1.5}\text{Fe}_{1.0}\text{-alloy}/(\text{MgO})_{3.5}$  ( $16.5 \text{ h}^{-1}$  at  $70^\circ\text{C}$ ),<sup>34</sup> and  $\text{NiFe/Cu}$  ( $35.3 \text{ h}^{-1}$  at  $70^\circ\text{C}$ )<sup>33</sup>). Figure 4(c) shows the conversion plots with/without using the HCl trap under 0.12 M NaOH. The conversion kinetics are almost same regardless of the HCl trap usage indicating that little ammonia is produced. In addition, the generated gases obtained during the decomposition reaction were analyzed by GC (Figure 4(d)). Figure 4(d) shows GC results before the injection of hydrazine solution and after the reaction of hydrazine decomposition, respectively. After reaction,  $\text{H}_2$  gas was detected. Importantly, no other peaks such as ammonia were detected except for  $\text{H}_2$  peak.

## Conclusion

In summary,  $\text{Co/MnO}$  was prepared by an annealing spinel  $\text{CoMn}_2\text{O}_4$  under hydrogen gas condition. In comparison to  $\text{CoMn}_2\text{O}_4$ ,  $\text{Co/MnO}$  catalysts exhibited the catalytic activity for the hydrazine decomposition and the 100%

selectivity for hydrogen. In addition, the catalytic activity of Co/MnO is higher than that of metallic Co under usage of same amount of catalysts. We believe that the improved catalytic property originated from the synergistic electric effect between metallic Co and MnO involved in charge transfer steps.

**Acknowledgments.** This research was supported by Basic Science Research Program through the National Research Foundation of Korea (NRF) funded by the Ministry of Education (NRF-2019R1I1A3A01059837) and by the Korea Basic Science Institute (KBSI) National Research Facilities & Equipment Center (NFEC) grant funded by the Ministry of Education (2019R1A6C1010042).

### References

1. J. A. Turner, *Science* **2004**, *305*, 972.
2. M. B. Ley, L. H. Jepsen, Y.-S. Lee, Y. W. Cho, J. M. Bellosta von Colbe, M. Dornheim, M. Rokni, J. O. Jensen, M. Sloth, Y. Filinchuk, J. E. Jørgensen, F. Besenbacher, T. R. Jensen, *Mater. Today* **2014**, *17*, 122.
3. J. D. Holladay, J. Hu, D. L. King, Y. Wang, *Catal. Today* **2009**, *139*, 244.
4. R. Lan, J. T. S. Irvine, S. Tao, *Int. J. Hydrog. Energy* **2012**, *37*, 1482.
5. T. C. Johnson, D. J. Morris, M. Wills, *Chem. Soc. Rev.* **2010**, *39*, 81.
6. M. Zheng, R. Cheng, X. Chen, N. Li, L. Li, X. Wang, T. Zhang, *Int. J. Hydrog. Energy* **2005**, *30*, 1081.
7. J. Prasad, J. L. Gland, *Langmuir* **1991**, *7*, 722.
8. A. A. Konnov, J. De Ruyck, *Combust. Flame* **2001**, *124*, 106.
9. P.-X. Zhang, Y.-G. Wang, Y.-Q. Huang, T. Zhang, G.-S. Wu, J. Li, *Catal. Today* **2011**, *165*, 80.
10. S. N. Oliaee, C. Zhang, S. Y. Hwang, H. M. Cheung, Z. Peng, *J. Phys. Chem. C* **2016**, *120*, 9764.
11. M. Liu, Y. Zheng, S. Xie, N. Li, N. Lu, J. Wang, M. J. Kim, L. Guo, Y. Xia, *Phys. Chem. Chem. Phys.* **2013**, *15*, 11822.
12. Z. Deng, X. Lu, Z. Wen, S. Wei, Y. Liu, D. Fu, L. Zhao, W. Guo, *Phys. Chem. Chem. Phys.* **2013**, *15*, 16172.
13. J. Wang, W. Li, Y. Wen, L. Gu, Y. Zhang, *Adv. Energy Mater.* **2015**, *5*, 1401879.
14. O. Song-Il, J.-M. Yan, H.-L. Wang, Z.-L. Wang, Q. Jiang, *Int. J. Hydrog. Energy* **2014**, *39*, 3755.
15. N. Firdous, N. K. Janjua, I. Qazi, M. H. Sarwar Wattoo, *Int. J. Hydrog. Energy* **2016**, *41*, 984.
16. L. He, Y. Huang, A. Wang, Y. Liu, X. Liu, X. Chen, J. J. Delgado, X. Wang, T. Zhang, *J. Catal.* **2013**, *298*, 1.
17. B. Xia, T. Liu, W. Luo, G. Cheng, *J. Mater. Chem. A* **2016**, *4*, 5616.
18. S. E. Colley, R. G. Copperthwaite, G. J. Hutchings, S. P. Terblanche, M. M. Thackeray, *Nature* **1989**, *339*, 129.
19. P. W. Menezes, A. Indra, N. R. Sahraie, A. Bergmann, P. Strasser, M. Driess, *ChemSusChem* **2015**, *8*, 164.
20. Y. Juan, S. Quaresma, M. Sen, J. M. F. Ferreira, P. Norby, *Key Eng. Mater.* **2005**, *280-283*, 713.
21. H. Chen, M. Yang, S. Tao, M. Ren, G. Chen, *Cryst. Growth Des.* **2016**, *16*, 6286.
22. V. A. De La Peña O'Shea, M. C. Alvarez-Galvan, J. M. Campos-Martin, J. L. G. Fierro, *Catal. Lett.* **2005**, *100*, 105.
23. C. Li, X. Han, F. Cheng, Y. Hu, C. Chen, J. Chen, *Nat. Commun.* **2015**, *6*, 7345.
24. W. Ni, S. Liu, Y. Fei, Y. He, X. Ma, L. Lu, Y. Deng, *J. Mater. Chem. A* **2016**, *4*, 7746.
25. Y. Su, Y. Zhu, H. Jiang, J. Shen, X. Yang, W. Zou, J. Chen, C. Li, *Nanoscale* **2014**, *6*, 15080.
26. D. P. Dubal, D. S. Dhawale, R. R. Salunkhe, C. D. Lokhande, *J. Electrochem. Soc.* **2010**, *157*, A812.
27. B. Liu, X. Hu, H. Xu, W. Luo, Y. Sun, Y. Huang, *Sci. Rep.* **2004**, *4*, 4229.
28. T. Kokubu, Y. Oaki, E. Hosono, H. Zhou, H. Imai, *Adv. Funct. Mater.* **2011**, *21*, 3673.
29. F. Dang, Y. Oaki, T. Kokubu, E. Hosono, H. Zhou, H. Imai, *Chem. Asian J.* **2013**, *8*, 760.
30. W. X. Yin, Z. P. Li, J. K. Zhu, H. Y. Qin, *J. Power Sources* **2008**, *182*, 520.
31. K. V. Manukyan, A. Cross, S. Rouvimov, J. Miller, A. S. Mukasyan, E. E. Wolf, *Appl. Catal., A* **2014**, *476*, 47.
32. S. K. Singh, Y. Iizuka, Q. Xu, *Int. J. Hydrog. Energy* **2011**, *36*, 11794.
33. S. K. Singh, A. K. Singh, K. Aranishi, Q. Xu, *J. Am. Chem. Soc.* **2011**, *133*, 19638.
34. L. He, Y. Huang, A. Wang, X. Wang, X. Chen, J. J. Delgado, T. Zhang, *Angew. Chem. Int. Ed.* **2012**, *51*, 6191.